63-3-2

WADD TR 61-91 Pt II

ULTRASONIC METHODS FOR NONDESTRUCTIVE EVALUATION OF CERAMIC COATING

TECHNICAL DOCUMENTARY REPORT NO. WADD TR 61-91
PART II

February 1963

Directorate of Materials and Processes
Aeronautical Systems Division
Air Force Systems Command
Wright-Patterson Air Force Base, Ohio

Project No. 7360, Task No. 736002

(Prepared under Contract No. AF 33(616)-6396
by the Armour Research Foundation of Illinois Institute of Technology
Chicago 16, Illinois;
K. E. Feith and W. E. Lawrie)

$1.50

NOTICES

When Government drawings, specifications, or other data are used for any purpose other than in connection with a definitely related Government procurement operation, the United States Government thereby incurs no responsibility nor any obligation whatsoever; and the fact that the Government may have formulated, furnished, or in any way supplied the said drawings, specifications, or other data, is not to be regarded by implication or otherwise as in any manner licensing the holder or any other person or corporation, or conveying any rights or permission to manufacture, use, or sell any patented invention that may in any way be related thereto.

Qualified requesters may obtain copies of this report from the Armed Services Technical Information Agency, (ASTIA), Arlington Hall Station, Arlington 12, Virginia.

This report has been released to the Office of Technical Services, U.S. Department of Commerce, Washington 25, D.C., in stock quantities for sale to the general public.

Copies of this report should not be returned to the Aeronautical Systems Division unless return is required by security considerations, contractual obligations, or notice on a specific document.

24-567C, 800, 4-11-63

FOREWORD

This report was prepared by the Armour Research Foundation of the Illinois Institute of Technology under USAF Contract No. AF 33(616)-6396. The contract was initiated under Project No. 7360 "The Chemistry and Physics of Materials," Task No. 736002, "Nondestructive Methods" The work was administrated under the direction of the Directorate of Materials and Processes, Deputy Commander / Technology, Aeronautical Systems Division, with Mr. Richard R. Rowand as project engineer.

This report covers work conducted during the period March 1, 1961 to February 28, 1962.

The ultrasonic investigations were conducted by K. E. Feith and W. E. Lawrie under the supervision of R. R. Whymark. Ceramic specimens, incorporating realistic defects were prepared by J. L. Bliton.

This work is a continuation of investigations reported in WADD TR 60-157 and WADD TR 61-91 Pt I.

ABSTRACT

This report describes investigations into the use of ultrasonic techniques to determine the strength and integrity of ceramic-metal bonds. An acoustic image converter system was used successfully to obtain a television type display of 1/32 inch diameter laminar defects in a zirconium oxide-inconel bond. The measured defect thickness varied between 300 and 500 microinches or about a factor of three greater than the average large grain in the coating material. Schlieren optical and acoustic lens techniques were used to visually investigate detailed properties of ultrasonic fields and the interaction of ultrasonic energy with a solid. The theory of Rayleigh waves was reviewed to provide a framework for experimental integrity determinations of ceramic coatings.

This technical documentary report has been reviewed and is approved.

W. J. TRAPP
Chief, Strength and Dynamics Research
Metals and Ceramics Laboratory
Materials Central

TABLE OF CONTENTS

LIST OF ILLUSTRATIONS

LIST OF ILLUSTRATIONS (Continued)

LIST OF SYMBOLS

SYMBOL	MEANING
p_{ii}	dilatational stress
p_{ij}	shear stress
λ	Lame' constant
μ	shear modulus
$\bar{S}$	particle displacement
u_i	component of particle displacement (u, v, w)
x_i	co-ordinates
$\bar{e}_i$	unit vector
ρ	density
θ	defined by $\bar{\nabla} \cdot \bar{S}$
ϕ	scalar displacement potential
$\bar{\Psi}$	vector displacement potential
α	velocity of dilatational wave
β	velocity of shear wave
k	wave number
c	trace velocity in x - direction
e	angle between interface and dilatational wave
f	angle between interface and shear wave
A	amplitude of dilatational displacement potential
B	amplitude of shear displacement potential

Section I

INTRODUCTION

Recent technological advancements have necessitated the exposure of metal structures to extreme environmental conditions capable of producing rapid failure of the structure through the processes of erosion and corrosion. In order to protect and prolong the life of these structures, ceramic materials are frequently applied to the metallic surfaces. Since the destructive environments sometimes consist of violent mechanical shock, high ambient temperatures, or possibly chemically active atmospheres, the strength and integrity of the coating-substrate system under such adverse conditions is of prime importance. Accordingly, the need arises for methods capable of detecting and evaluating possible defects in the ceramic-metal bond prior to the exposure of the coated surface to the destructive environment.

The objective of this program has been to develop nondestructive ultrasonic techniques capable of determining the strength and integrity of coating-metal substrate systems. This report covers investigations conducted during the third year of the project. The first years work[1] explored many different techniques in an effort to discard those not obviously applicable. During the second year,[2] those methods that showed greatest promise of success, i.e., intermodulation, charge scanning, direct transmission, and surface wave propagation, were investigated in greater detail. Current work has been primarily concerned with further developing several of the above mentioned techniques, to a point where they can be used for the examination of practical systems.

Two dimensional displays have been obtained of 1/8, 1/16 and 1/32 inch diameter laminar defects formed at the bond of a 0.003 inch thick zirconium oxide coating flame-sprayed onto inconel. An acoustic image converter system was used as the detector. The defects are formed by new techniques (Section II) and simulate very closely the defects that might arise in manufacture, or during exposure to adverse environments, of practical systems. The defect thicknesses varied from 0.0003 to 0.0005 inch or about three times larger than the average coarse grains observed by photomicrography of the zirconia. The imaging system is based on an

---

[1] The results of the first years work are presented in WADD Technical Report 60-157.

[2] The results of the second years work are discussed in detail in WADD Technical Report 61-91, Part 1.

Manuscript released by author 28 February 1962 for publication as a WADD Technical Documentary Report.

acoustic image converter tube, similar to a television camera tube with the exception that the photosensitive surface is replaced by piezoelectric material. Its principle of operation is analogous to that of the charge scanning technique[3] (Section II).

Certain types of coating-substrate systems present high loss mechanisms to the acoustic waves. By using acoustic lenses, high acoustic intensities can be produced in the incident sound beam so that an adequate signal to noise ratio is obtained at the detector in spite of high absorption of the specimen. To study the focussing properties of suitable plastic lenses, a Schlieren optical system (Section III) is used, which also serves the valuable function of providing a visual image of the interaction of the focussed sound beams with the metal specimens. It is important that sound fields of known characteristics be employed and the Schlieren system has been proven to be capable of giving detailed information of such properties.

The increased emphasis on the inspection of diffusion coatings has renewed interest in surface wave techniques. The theory of surface waves has been reviewed (Section IV) and the theory has provided a better understanding of the generation and propagation of surface waves. The theory has also provided guidance to the experimental program, and the understanding of the properties of surface waves has helped in designing experimental techniques and interpreting results.

The most common type of failure of diffusion coating-substrate systems is the formation of cracks normal to the surface, with subsequent bond failure, in some cases, as a result of stresses exerted through the formation of oxides. Experimental techniques are being developed to detect these cracks through measurements of surface wave attenuation. Surface waves are generated in the diffusion coated specimen using a lucite wedge transducer, and after propagation along the surface for a distance dependent upon the length of the specimen submerged in water, are reconverted to compressional waves for detection. Initial experiments gave spurious results. Redesign of the lucite wedge transducers to prevent the generation of shear and compressional waves in the specimen have eliminated the spurious responses and attenuation measurements are now being made.

Section II

ACOUSTIC IMAGING

One of the more effective detection methods, using direct transmission of sound energy, is the charge scanning technique. This method was used extensively during the second years work to obtain visual images of sound shadows produced by simulated defect structures in metal plates.

---

[3] WADD TR 61-91, Part 1, page 4.

In the course of exploiting this method of defect detection, a new technique was used, whereby the detecting device is very similar to a closed circuit television system. This technique has produced visual images of 1/32 inch diameter simulated defects in coating-substrate systems in which the defect thickness is only a factor of three larger than the average coarse grains found in the coating material.

CHARGE SCANNING

In a previous technical report,[3] the concept of "piezoelectric charge scanning" was presented in detail. This technique utilizes the piezoelectric properties of a quartz crystal and the crystals spatially independent response to variations in the sound pressure incident upon its surface, to produce two dimensional visual images of sound shadows. To illustrate this technique, one might consider the case where ultrasonic energy is transmitted through a solid material having a defect present in the transmission path. The sound pressure at any point on a cross section of the emergent sound beam will be dependent upon the transmission coefficient of a corresponding point in the solid. If a quartz crystal is placed near to and parallel with the surface of the solid, a piezoelectric charge distribution will be developed on the back side of the crystal. This charge distribution closely simulates the sound pressure distribution incident upon the crystals front surface and thus indicates spatial variations in the transmission coefficient of the material under test. If a small mechanical probe is moved across the back surface of the detecting crystal, a voltage is obtained that varies with the spatial changes in the incident sound pressure. This voltage is then used to control the intensity of a cathode ray tube electron beam. Through appropriate circuitry, the electron beam can be made to move in synchronism with the probe. Therefore, by moving the probe across the crystal at given increments, a visible image of the defect geometery is produced on the face of the cathode ray tube.

Early experiments with the charge scanning apparatus were very encouraging. The system exhibited sufficient acoustic resolution and sensitivity to detect a 0.030 inch diameter simulated defect in a 1/4 inch thick steel plate. However, the operation of the apparatus was somewhat limited in that only a small area (approximately 0.5 square inches) could be scanned. Furthermore, since the scanning was performed manually, the operation was slow and tedious, taking anywhere from ten to fifteen minutes to cover a 3/4 inch diameter area.

ACOUSTIC IMAGE CONVERTER

Recently, an expeditious form of charge scanning has become available in the laboratory at A.R.F. This new device, known as an "acoustic image converter tube", operates along the same general

---

[3] loc. cit.

principles as the charge scanner discussed above. However, the converter utilizes an electron beam probe and secondary electron emission from a quartz crystal to produce a two dimensional image of a defect structure.

The image converter tube is analogous to a television camera tube in which the photosensitive surface is replaced by a piezoelectric or ferroelectric material. A simplified line drawing of the tube and its operation is shown in Fig. 1. In the image converter system discussed here, the transducer elements are 1.5 inch square, 7 Mc/s, x-cut quartz crystals which provide an active area of approximately two square inches. As in the charge scanner, through the piezoelectric characteristics of the quartz, the spatial sound pressure variations over a cross section of an incident sound beam are converted to charge density variations over the ungrounded surface of the detecting crystal. This surface is continually scanned in two dimensions by a 500 volt electron beam, and secondary electrons are emitted from the quartz. These secondary electrons, collected by an appropriate electrode near the quartz surface, produce an alternating current which has the same frequency as the transmitted ultrasonic energy. The amplitude of this current is proportional to the incident sound pressure at the point on the crystal where the secondaries were emitted. The resulting spatially varying signal, after amplification and detection, is used to control the beam intensity of a display cathode ray tube. If the sweeps of the image converter and display tubes are synchronized, one will obtain a television type display of the sound shadow produced by a defect in the material under investigation.

EXPERIMENTAL METHOD

The acoustic image converter system was investigated to ascertain its ability to detect small defects in ceramic-metal bond structures. In order to obtain a true evaluation of the apparatus, it is desirable to experiment with specimens that possess known bond defects. During previous investigations, simulated defects were produced in a number of different ways[4] i.e., drilling and plugging holes in the substrate material prior to coating. Although several of these methods produced satisfactory defects, they were not indicative of the type of bond defect normally encountered in practice. In an effort to obtain realistic defect structures, several new techniques have recently been developed. As a result, three types of bond defects were produced that exhibit the same geometrical and physical properties as those encountered in practice. Listed below are the methods used to produce defects at the interface of ceramic-metal bonds.

---

[4] WADD Technical Report 60-157, page 11 and WADD Technical Report 61-91, Part I, page 16.

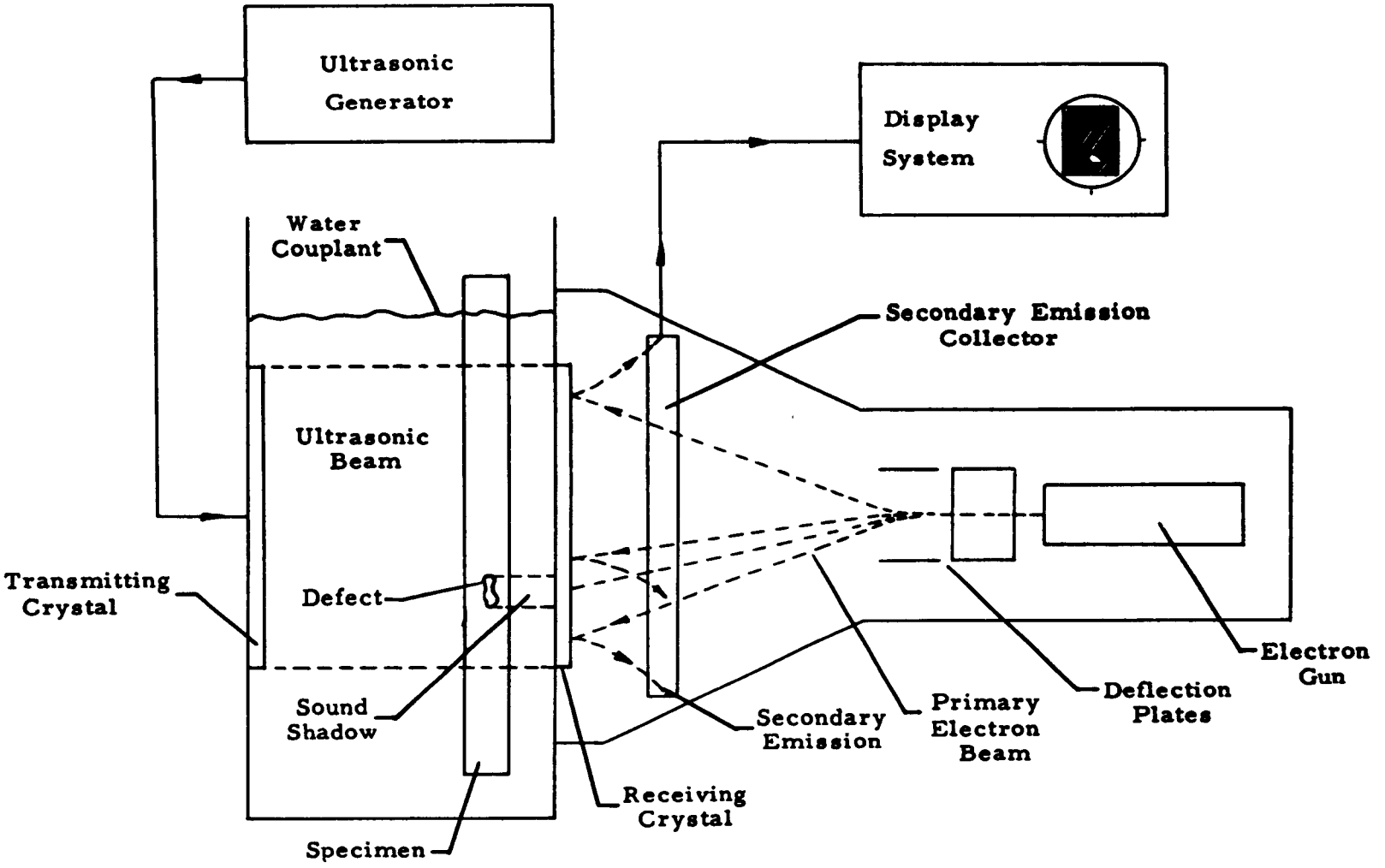

Fig. 1 - ACOUSTIC IMAGE CONVERTER SYSTEM.
The piezoelectric potential variations, caused by spatial variations in sound pressure, produce changes in the AC component of the secondary emission from the receiving crystal. The secondary electrons, gathered by the collector, provide an output current which is used to generate a two dimensional image on the display oscilloscope.

Masked Defect

This type of defect was produced by masking a small area on the surface of the substrate material before exposing it to a sandblasting process.[5] The masking material is then removed and the surface of the specimen is cleaned with a suitable solvent. When a flame-sprayed coating of zirconium oxide is applied to the surface, an integral bond is not obtained over the area that was masked, hence, a known size defect is obtained at the ceramic-metal interface.

Grease Spot Defect

Another form of defect was produced by applying a known size spot of grease to the sandblasted surface of the substrate prior to coating. The resulting defect structure at the ceramic-metal interface closely simulates a typical defect found in practice, only its size can be controlled.

Sodium Chloride Defect

To obtain a "clean" defect between the metal and its ceramic coating, which is analogous to an air pocket, a globule of sodium chloride solution was evaporated on the sandblasted surface. Upon completion of the coating process, the surface of the specimen was washed with water. Due to the porosity of the zirconium oxide coating, the sodium chloride grains go into solution and the defect structure is left clean. As one might expect, it is very difficult to control the defect size when using this procedure, however, the technique is still representative of typically encountered defects.

Several specimens were prepared using the above techniques. The substrate material is 1/8 inch thick inconel plate with approximately 0.002 to 0.003 inch coatings of flame-sprayed zirconium oxide. Each plate contains three defects, 1/8, 1/16 and 1/32 inch in diameter, with the exception of the plate containing the sodium chloride defects which are somewhat larger.

Preliminary experiments with the image converter showed that close geometrical tolerances had to be maintained, between the converter face and the specimen, to reduce spurious indications of defect size and

---

[5] The surface of a substrate material is normally sandblasted with 20 grit silicon carbide at a pressure of 80 psi, before a flame-sprayed ceramic coating is applied.

configuration. A special sample holder, Fig. 2, was constructed to hold the specimen normal to the sound beam and maintain a constant 1/16 inch spacing between the specimen and image converter faces as seen in Fig. 3. The specimen is placed between the guides of the holder and slowly moved into the ultrasonic beam. The emergent sound beam is continually scanned, as described earlier, and the resulting image is monitored on the display unit.

EXPERIMENTAL RESULTS

Experimental results are presented in the photographs described below of the converter display system. Each pair of scans, noted by their overlap, are of the same defect. However, the upper image was obtained with the transmitted sound incident upon the ceramic coating while in the lower image, the uncoated side was exposed to the incident sound beam. The sensitivity of the image converter system was held constant for each pair of images so as to determine the effect of the zirconia coating on the incident sound.

Figure 4 shows sound images of the 1/8, 1/16 and 1/32 inch defects produced by the masking technique. Figures 5 and 6 are images of the three defects produced by the grease spot and sodium chloride methods respectively. It will be noted that in general, the image of the bond defect is better defined when the specimen is examined with its zirconium oxide surface towards the inciden sound beam. This effect is explained by considering the sound absorption and scattering properties of the coating material. When the sound beam propagates through the zirconia layer, a portion of its energy is absorbed and the remainder scattered in some random fashion. However, the sound energy that emerges from the zirconia layer will produce a relatively uniform sound field over the interface. It is this sound energy, that has already undergone attenuation and scattering, that sees the defect structure in the ceramic-metal bond. Experiments have shown that the metal substrate produces only negligible scattering, hence the geometery of the shadow produced by the defect is essentially unperturbed.

If we now reverse the specimen so that the incident sound is propagated through the metal substrate first, it is immediately apparent that the sound shadow, produced by the defect, will be affected or possibly obliterated, before it reaches the detecting crystal, due to the scattering properties of the zirconium oxide. This effect is apparent in the images of 1/16 and 1/32 inch defects and will be clearly demonstrated by Schlieren experiments discussed in Section III.

To ascertain the minimum defect thickness that is detectable with the acoustic image converter system, the specimen, containing defects produced by the masking technique, was sectioned through its 1/8 inch diameter defect. The surface of the section was etched with 5 percent H_2SO_4

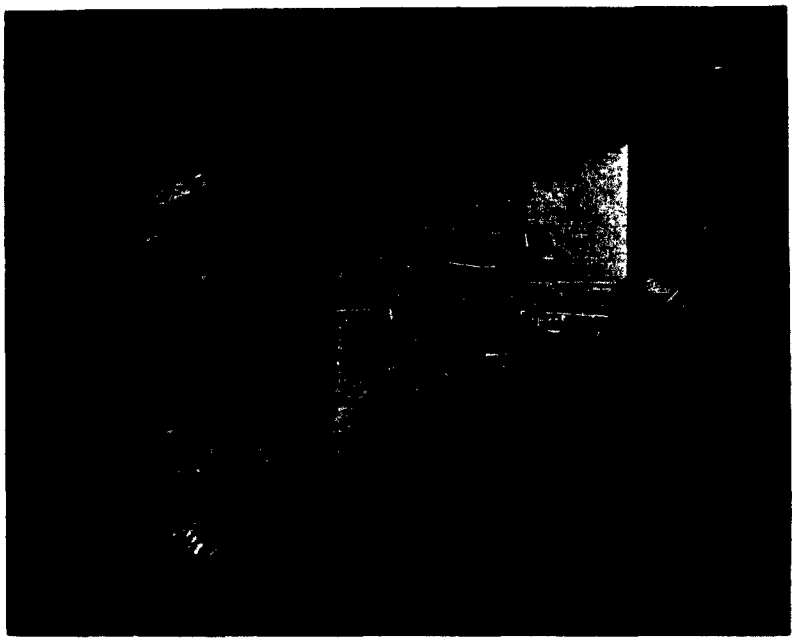

Fig. 2 - PRECISION SAMPLE HOLDER. This holder maintains the required parallelism between the sample and the image converter face.

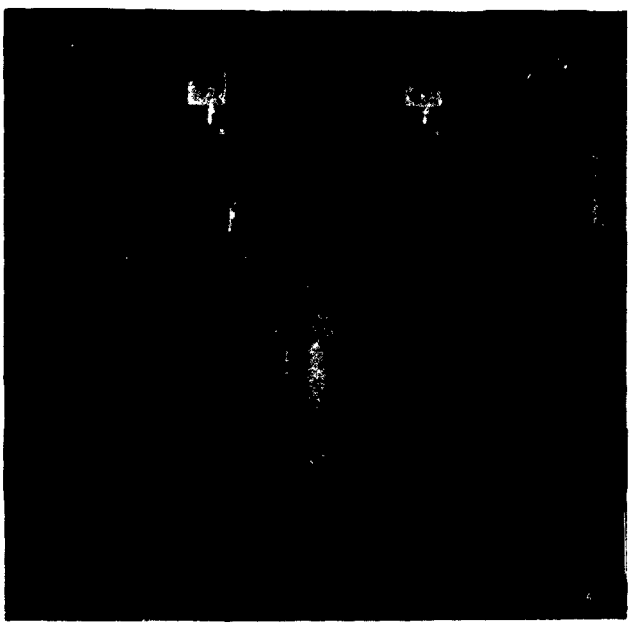

Fig. 3 - TANK ASSEMBLY OF IMAGE CONVERTER. The tank is normally filled with water to provide acoustic coupling between the transmitter assembly, seen in the foreground and the image converter face, seen in the background. The sample holder is shown in place immediately in front of the converter face.

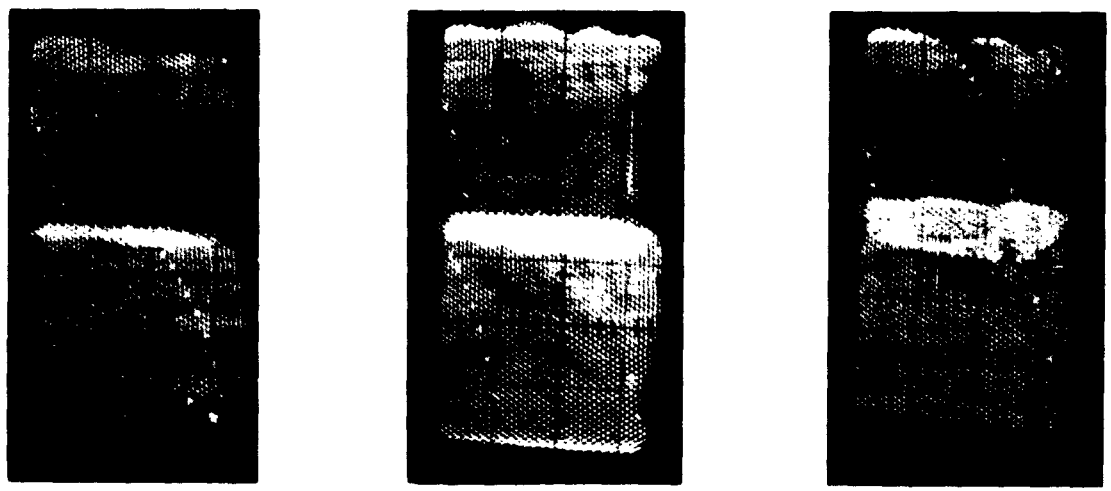

Fig. 4 - ULTRASONIC IMAGES OF SIMULATED MASKED DEFECTS IN ZIRCONIUM OXIDE - INCONEL BOND. The defects were produced by masking an appropriate surface area of the substrate before sand-blasting. The masking was then removed and a zirconium oxide coating applied to the entire surface. The small dark spot located to the right of the 1/8 inch defect, is produced by a scratch in the coating material.

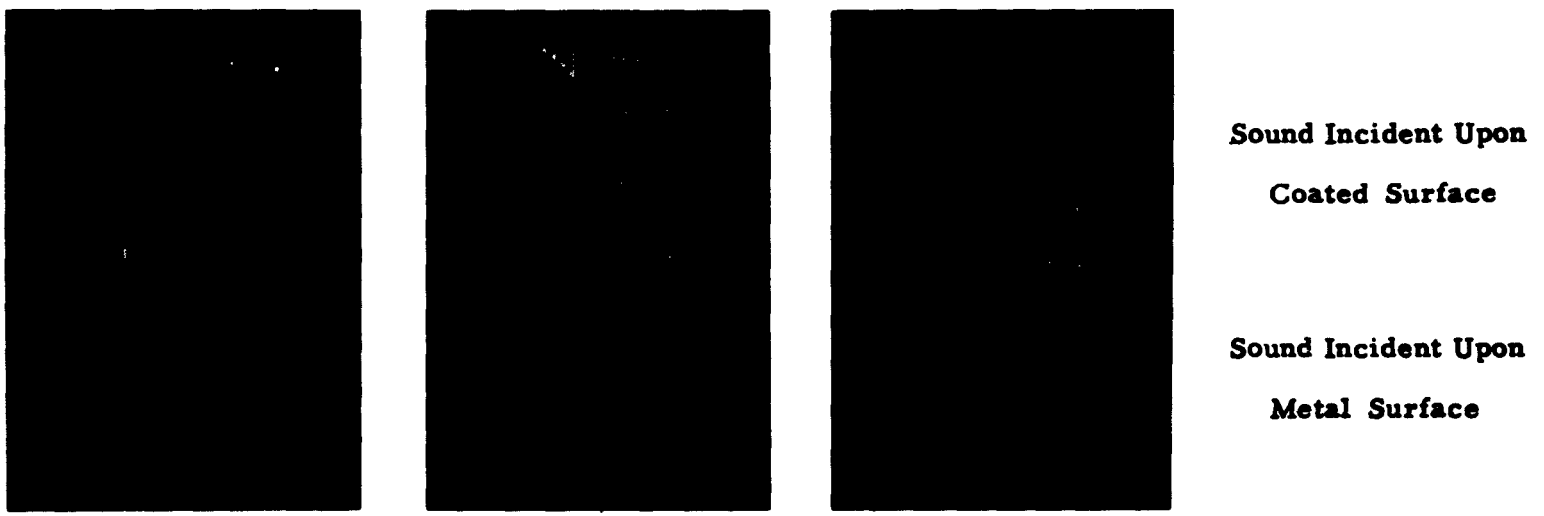

Fig. 5 - ULTRASONIC IMAGES OF SIMULATED GREASE DEFECTS IN A ZIRCONIUM OXIDE - INCONEL BOND. The defects were produced by depositing a given size grease spot on the sandblasted surface of substrate. The zirconia coating was applied over the grease to produce the defects shown.

Fig. 6 - ULTRASONIC IMAGES OF SIMULATED DEFECTS, PRODUCED BY SODIUM CHLORIDE, IN A ZIRCONIUM OXIDE - INCONEL BOND. These defects were produced by evaporating a sodium chloride solution on the sandblasted substrate surface. A zirconium oxide coating was then applied. The specimen was then immersed in water to dissolve the sodium chloride crystals.

and a photomicrograph, using a magnification of 250X, was taken of the defect and its adjacent bond structure. Figure 7 shows the defective bond structure as a black strip between the zirconium oxide and the inconel substrate. The substrate surface in this area is relatively flat due to lack of sandblasting. Measurements show the defect thickness to be between 0.0003 and 0.0005 inches or about a factor of three times larger than the average coarse grains in the zirconia coating. A typical bond structure, showing good integrity was obtained adjacent to the defect and is shown in Fig. 8. It will be noted that the substrate surface in this area is coarse due to sandblasting prior to application of the zirconium oxide coating.

Diffusion type coatings were not examined with the acoustic image converter due to the geometrical configuration of their defects. In general, the defect structures are in the form of cracks which traverse normal to the surface. Metallographic examinations have shown these cracks to be about 250 microinches wide with a surface penetration of approximately 0.003 inches. In view of the above mentioned defect thicknesses that are detectable with the image converter, it may be feasible to use this method or a variation of this technique to detect cracks in vapor-deposited coatings.

Section III

SCHLIEREN OPTICAL AND ACOUSTIC LENS SYSTEMS

The inspection of solids, using ultrasonic techniques, depends upon the interaction of the sound beam with the solid. Although the rules of geometrical optics and a knowledge of the elastic properties of the solid permit analytical predictions of the interaction, in general, the inherent imperfections in the detecting system and specimen limit the applicability of theoretical treatments.

Previous investigations of ultrasonic testing techniques have produced several new and promising methods, e.g. charge scanning and acoustic image conversion, for the detection of defects in solids. Although these techniques have proved their ability to resolve small defect structures in various materials, confusion is frequently encountered in analyzing the test results. This confusion is produced by the non-uniform sound fields generated by the transducers and also by interaction phenomena produced at the solid interfaces.

If defect structures of small dimensions are to be detected with reliability, sound fields of known detailed properties must be employed.

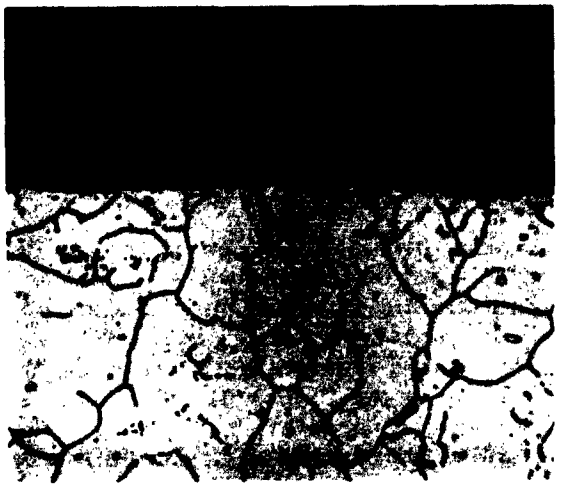

Fig. 7 - PHOTOMICROGRAPH OF TYPICAL 1/8 INCH DIAMETER LAMINAR DEFECT IN A ZIRCONIA-SUBSTRATE SYSTEM. The dark area between the zirconium-oxide and inconel substrate is a 250x magnification of a 0.0005 inch thick bond defect. The defect was produced by masking the surface prior to sandblasting.

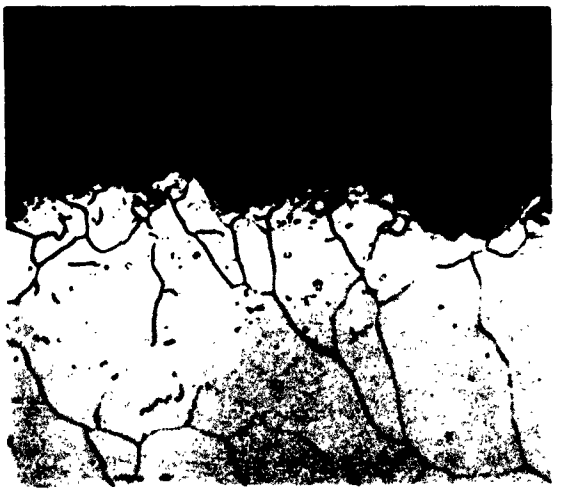

Fig. 8 - PHOTOMICROGRAPH OF TYPICAL ZIRCONIUM OXIDE - INCONEL BOND. The section shown is adjacent to the 1/8 inch defect. The coarse surface of the substrate was produced by sandblasting before applying 2 - 3 mil of zirconia.

To obtain a more comprehensive understanding of ultrasonic fields and interaction phenomena, it is necessary to study, in detail, the propagation of compressional waves in both liquids and solids. Quantitative measurements of these parameters are frequently a formidable task and are equally difficult to analyze. A more direct approach is a qualitative study using visual inspection and evaluation of the sound beam and its associated effects.

The Schlieren optical system provides a very sensitive method[6] for visual investigations of compressional wave propagation. Theory shows that successive compressions and rarefactions of a sound beam alter the indices of refraction of the medium in which it travels. If the medium is transparent, e.g., water, and a collimated beam of light is caused to traverse the sound beam at right angles, the light will effectively see a sinusoidal diffraction grating. Consequently, some of the light will be diffracted away from the primary light beam and a diffraction pattern, as shown in Fig. 9, is observed. In a Schlieren system, the primary collimated light beam is intentionally obscured since it is the diffracted light that produces the visual image of the sound beam. In general, the visual image of the sound beam is composed of various shades of light. These variations in light intensity correspond to variations in the sound field, where the bright and dark areas indicate high and low sound intensities respectively. Advantages are obtained through the use of this method in that its adjustments are essentially independent of ultrasonic frequency. Furthermore, the wave propagation is unaltered by the detection system. On the contrary, most other methods such as calibrated probes, require critical adjustments for each new frequency and geometrical location in the sound field and, hence, could present additional perturbations in the measurements.

Previous investigations have shown that some materials present high loss mechanisms to the acoustic wave, therefore, higher acoustic intensities are required in the incident sound beam. By introducing an ultrasonic lens system to focus the sound energy, high intensity ultrasonic radiation is obtained with a corresponding decrease in beam cross section. The reduction in sound beam area produces improved resolution of small defect structures. The lens system can be accurately adjusted, relative to a specimen, by viewing the incident and emergent focussed sound beams with the Schlieren optical system.

---

[6] "Sonics" Hueter and Bolt, John Wiley and Sons, New York, N. Y. page 349.

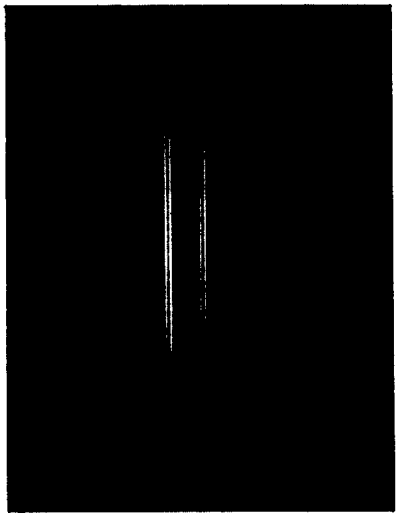

Fig. 9 - DIFFRACTION PATTERN PRODUCED BY A 7MC/S ULTRASONIC BEAM. The primary light has been "stopped" since in a Schlieren system the diffracted light produces a visual image of the sound beam.

EXPERIMENTAL METHOD

The experimental apparatus, shown in Fig. 10, incorporates two ultrasonic transducers (one acting as a generator, the other as a receiver) mounted on a precision base plate to maintain their necessary parallelism. The transducers are constructed to allow their complete submersion in a liquid. The active element in each unit is a one inch square, 7 Mc/s, x-cut quartz crystal. The capacitive reactance of the crystals is tuned out by means of a variable series inductance. Hence, when properly tuned to their resonant frequency only the low resistive component of the crystal impedance is seen by the ultrasonic generator. This resistance is somewhat lower than the output impedance of the ultrasonic power oscillator; however, sufficient voltage is developed across the crystal to generate a strong ultrasonic beam.

The entire assembly is submerged in a water filled tank that has two 6 inch diameter, optically flat and parallel, glass portholes. A collimated light beam is caused to pass through these glass ports, traversing the sound beam at normal incidence. The emergent light is then processed, as discussed above, and a visual image of the wave propagation in the water media is projected on a screen by use of an optical lens.

Experiments have shown that when a homogeneous steel plate is placed in an ultrasonic beam, as shown in Fig. 11, the sound fields on both the incident and emergent sides of the specimen are diffuse. This phenomenon is attributed to imperfect collimation of the incident sound beam and/or lack of parallelism between the sound generator and the specimen.

When a compressional wave is propagated through a solid, a portion of the sound energy is reflected at the water-solid interface due to a change in acoustic impedance. If the sound beam is well collimated and intersects the solid at normal incidence, the reflected energy will travel back along its incident path. However, in the case of a poorly collimated beam, sound energy will be reflected at random angles and appear well away from the primary sound beam. In a similar manner, refraction of the uncollimated portion of the sound beam can produce a diffuse emergent sound beam due to reverberation within the solid. Furthermore, if the sound energy is poorly collimated or if the solid is not normal to the sound beam, through the process of mode conversion at the liquid-solid interface, shear components can be produced within the solid. These shear waves can, by double mode conversion, reradiate compressional components back into the liquid at random angles. The above interactions are best illustrated by the line drawing of Fig. 12.

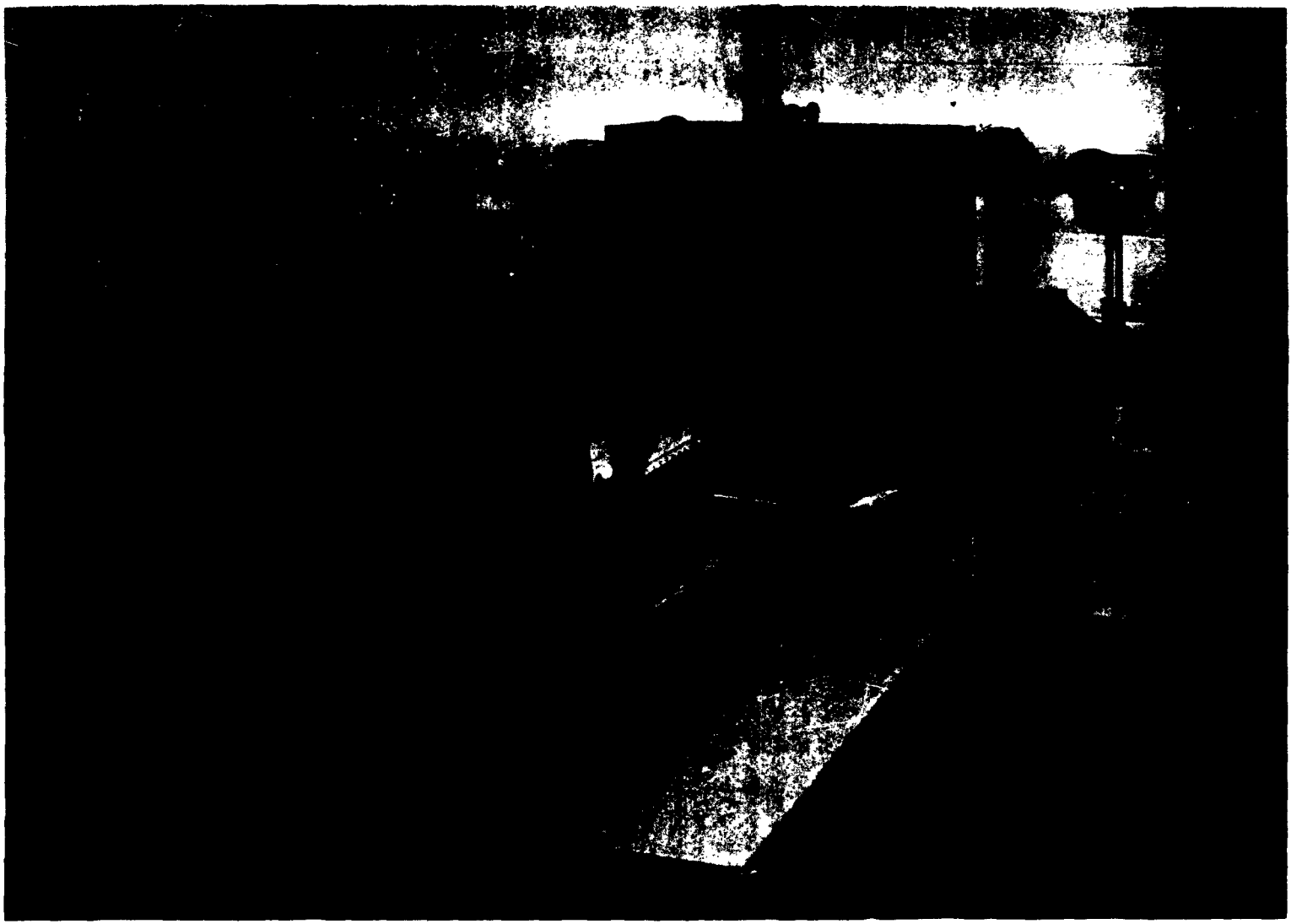

Fig. 10 - SCHLIEREN OPTICAL SYSTEM. The acoustic lens system and specimen are submerged in the water tank. A collimated light beam is passed through the portholes of the tank. The resultant acoustic image is projected on a screen by the optical lens shown to the right of the system.

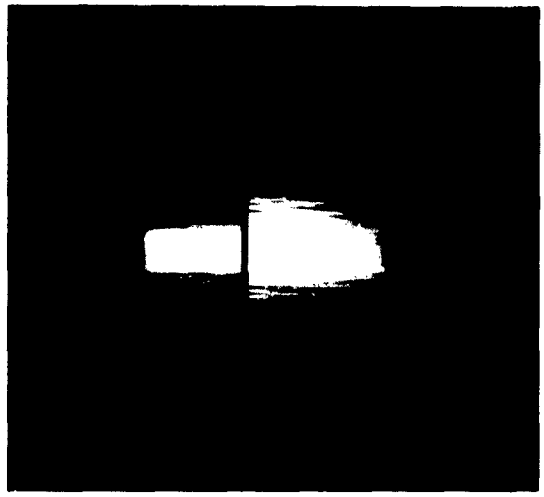

Fig. 11 - THE INTERACTION OF A POORLY COLLIMATED SOUND BEAM WITH A HOMOGENEOUS STEEL PLATE. It will be noted that not all of the diffuse sound, incident upon the right side of the plate, is transmitted. Furthermore, many of the reflections seen in the incident sound beam are produced by poor parallelism between the plate and sound generator.

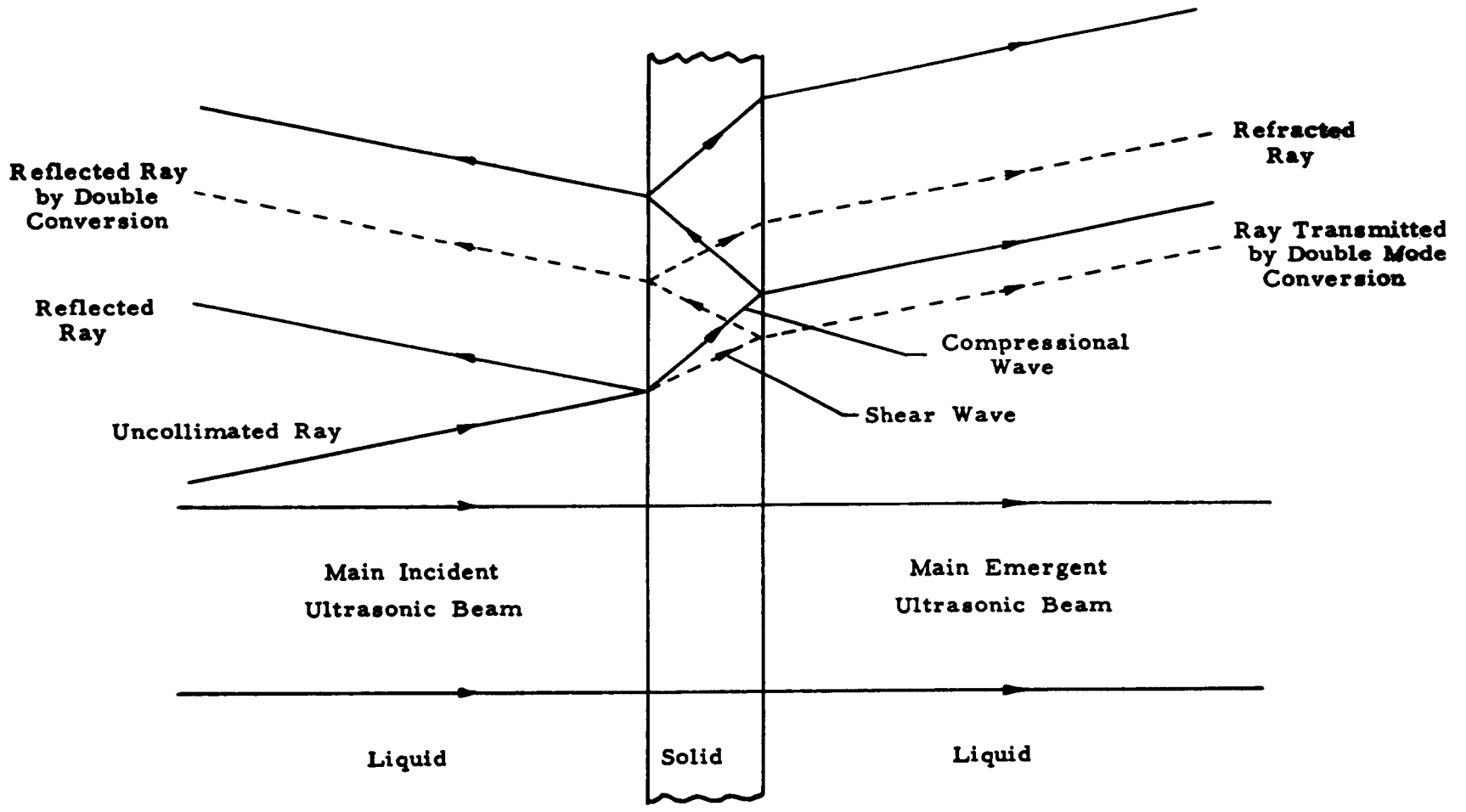

Fig. 12 - DIFFUSE SOUND FIELD PRODUCED BY POOR COLLIMATION OF ULTRASONIC BEAM.

ACOUSTIC LENSES

As mentioned previously, scattering and attenuation of sound energy occurs upon emergence from solids, if certain acoustic and geometric considerations are not fulfilled. In general, it is not possible to obtain optimum acoustic and geometrical conditions, which depend in part upon the specimen e.g., zirconium oxide on steel.

Through the use of an acoustic lens, a means is provided whereby most of the transmitted ultrasonic energy is concentrated into a beam of very small cross sectional area. In so doing, high sound intensities are produced over a very small region of a specimen. Any defect that is present in this region will appear to be magnified, since it will now occupy a larger fraction of the cross sectional area of the beam. Furthermore, the higher sound intensity enables us to examine materials which exhibit high sound absorption.

Two planoconcave lenses, 2.5 inches in diameter, were constructed of polystyrene. This material was selected because of its relatively low sound absorption coefficient. They were designed to have a 1.5 inch radius of curvature which produces a focal length of 4.0 inches. The lenses were mounted on the precision base plate, Fig. 13, with their plane surfaces toward and parallel with each transducer element. Provision was made to allow movement of each lens in a direction parallel with the sound beam, so that their focal points can be adjusted through a distance of about one inch.

The specimen is mounted on a traverse mechanism, located midway between transducers, which allows both horizontal and vertical motion of the specimen in a plane normal to the sound beam. Hence, the sound beam from the transmitting quartz is focussed, by means of the lens, so as to embrace only a small area of the specimen at any one time. On emergence from the specimen, the sound energy passes through the second lens and is received by the quartz crystal in the detecting circuit. The presence of a defect is indicated by a sharp drop in the received signal amplitude. By the use of the mechanical traverse mechanism, the specimen can be moved in a plane normal to the sound beam. Hence, a series of magnified images of the defect structure, as a function of geometrical location, can be obtained. Use of the lens system in conjunction with the Schlieren optical equipment permits electronic and optical detection simultaneously. The operation of the lens system is illustrated in Figs. 14 and 15. Figure 14 shows the transmitted sound beam (approximately one inch square) incident upon the plane surface of the lens and the resulting focussed energy. In Fig. 15, the lens is out of view, however, the crossover at the focal point of the lens is clearly demonstrated. Some aberration of the focussed sound beam is observed which is partially due to poor collimation of the transmitted energy. Also, in lenses having a small radius of curvature, aberrations are more pronounced when the whole lens area is used. By use

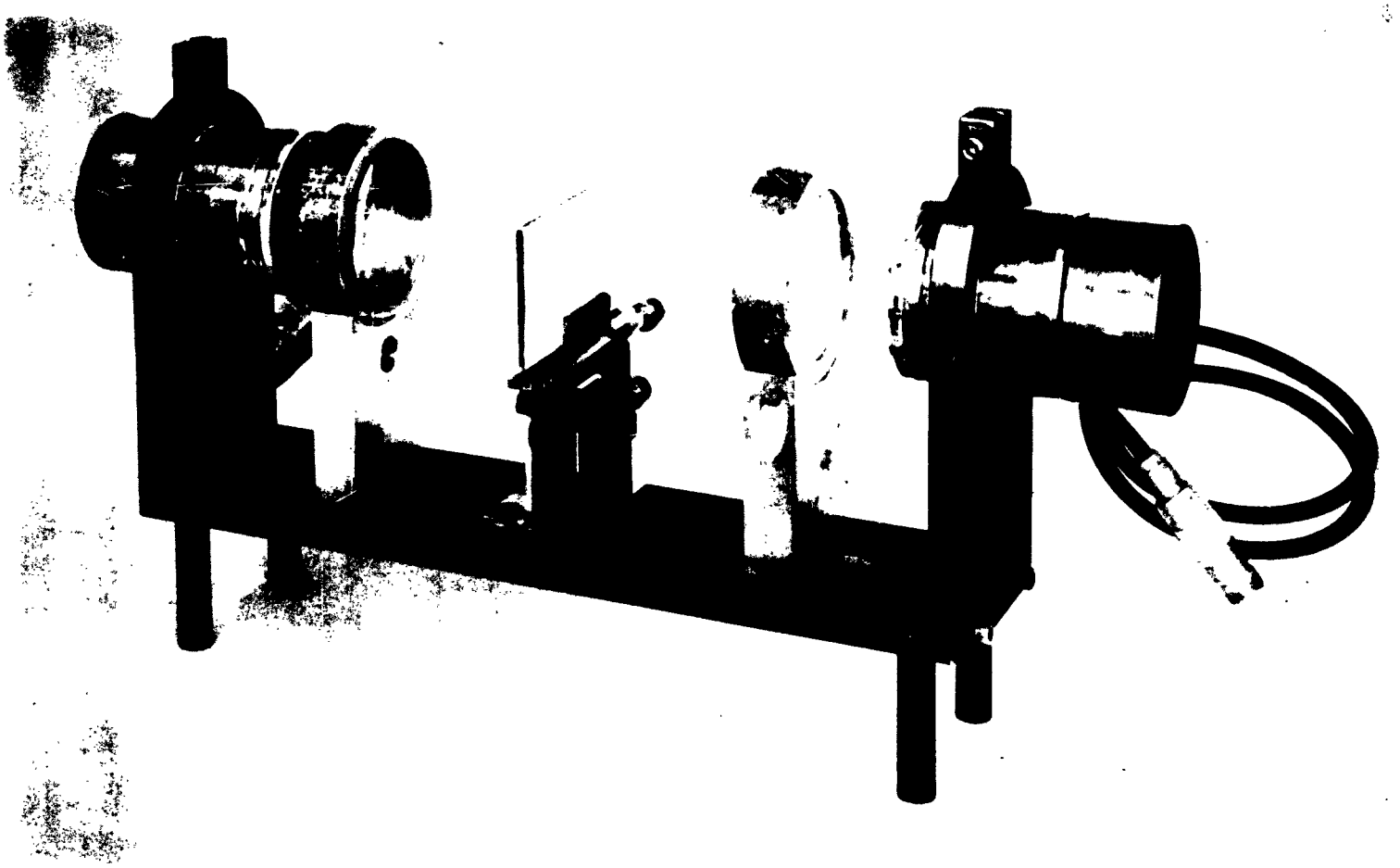

Fig. 13 - ACOUSTIC LENSES. The lenses are mounted with their plane surface toward and parallel with each transducer element. The specimen traverse mechanism, located midway between transducers, is horizontally and vertically adjustable. The focal point of both lenses is adjustable over one inch.

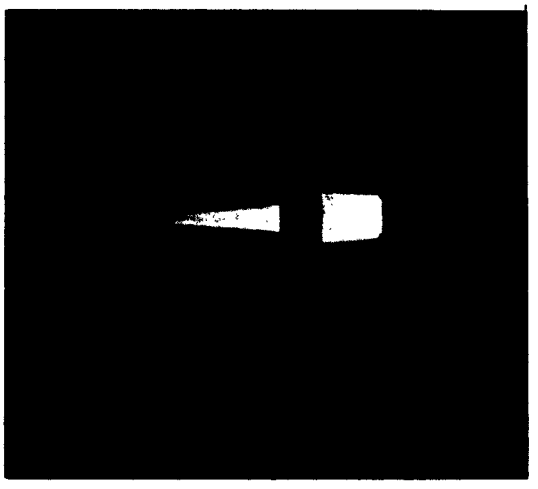

Fig. 14 - FOCUSSING ACTION OF ACOUSTIC LENS. The incident beam, approximately one inch square, is poorly collimated, consequently spreading of the focussed sound is observed. The direction of propagation is from right to left.

Fig. 15 - CROSSOVER PRODUCED AT THE FOCAL POINT OF AN ACOUSTIC LENS. A zone of confusion is clearly discernable at the plane of focus due to the effect of diffuse sound.

of an appropriate acoustic aperture the active area of the lens can be reduced which will result in a corresponding reduction of aberration. It should be pointed out that the Schlieren system was adjusted for maximum sensitivity in Fig. 15. Consequently, most of the refracted and reflected components of the primary sound beam are discernable. If the sensitivity of the optical apparatus is slightly reduced, these secondary effects diminish and a sharp focal point is produced.

EXPERIMENTAL RESULTS

The operation of the acoustic lens and Schlieren optical systems has been discussed in detail above. Through the use of these apparatus, a qualitative analysis, of the interaction of compressional waves with a solid, was conducted. To evaluate the experimental data, acoustic energy loss mechanisms must be considered. The primary loss mechanisms inherent in most solids are: scattering, heat conduction, elastic hysteresis, and viscous friction. A complete dissertation on these mechanisms is not warrented at this time, however, these energy "sinks" do have a significant effect on the following experimental results.

When compressional waves are propagated through a solid, the intensity of the emergent sound beam is governed by the attenuation within the material and the reflection coefficients at its interfaces. The reflection coefficient, in turn, is related to the acoustic impedance mismatch at the couplant-solid interface and follows conventional transmission line theory. For our investigations, various metallic materials were placed at the focal point of the sound beam. By adjusting the electronics for maximum transmitted sound energy, the impedance is optimized and the intensity of the emergent sound beam is essentially controlled by only the attenuation within the solid. A qualitative comparison of sound beam configurations for these various materials enables one to rank order the specimens as to their sound absorption or attenuation characteristics.

To avoid confusion, each specimen will be discussed separately and comparisons made when necessary. Furthermore, it should be noted that in all subsequent figures, the direction of wave propagation is from right to left.

Aluminum

The first material examined was a 1/4 inch thick aluminum plate. The Schlieren photograph of Fig. 16A clearly indicates the low sound absorption of aluminum. The emergent beam configuration is essentially what one would predict from

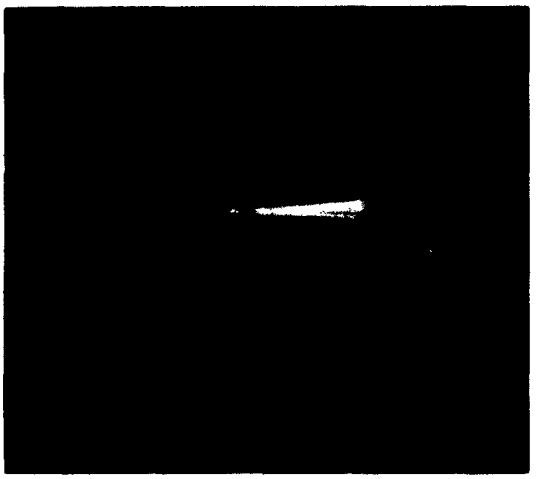

(A) 1/4 Inch Thick Aluminum Plate

(B) Diffusion Coating of Chromalloy W2 on 1/4 Inch Thick Molybdenum Plate

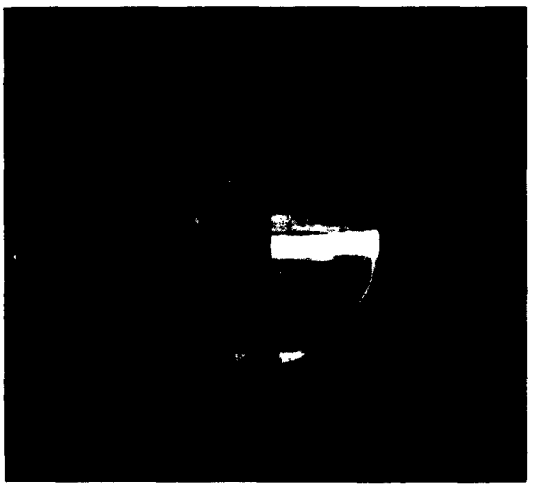

(C) 1/4 Inch Thick Lead Plate

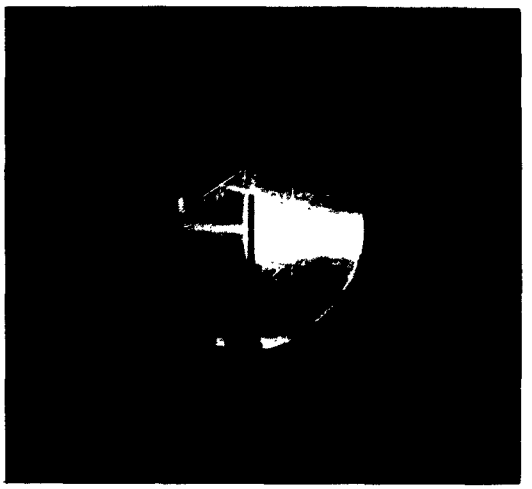

(D) Zirconium Oxide Coating on 1/8 Inch Thick Steel Plate. Coated Surface is to the Left.

Fig. 16 - QUALITATIVE COMPARISON OF SOUND ATTENUATION IN VARIOUS MATERIALS. 7 Mc/s sound energy was propagated from right to left and focussed at a plane midway between the surfaces of each specimen. In each case the emergent sound was adjusted for maximum intensity.

theory. Due to the relatively high sound velocity in this material, as compared to that in water, the angle of refraction is large, hence, the transmitted beam appears wide at its point of emergence from the plate. Although there are indications of diffused sound being present, it will be noted that the emergent beam is not significantly altered by it.

Chromalloy W2 on Molybdenum

A diffusion coating of Chromalloy W2 on a 1/4 inch thick molybdenum plate is shown in Fig. 16B. By comparing the emergent beam with that observed in Fig. 16A for aluminum, it is obvious that this specimen presents greater loss mechanisms to the sound beam and therefore has a greater sound absorption than does aluminum. Again, due to the higher sound velocity in this material, the transmitted beam appears to widen at its point of emergence.

Lead

Figure 16C illustrates the sound transmission properties of a 1/4 inch thick lead plate. Since the velocity of sound in lead is nearly the same as in water, the transmitted sound energy is hardly affected by refraction effects within the plate. Hence, if the emergent beam is projected back into the plate, its focal point would almost coincide with that of the incident beam. It is quite evident that the lead plate presents high attenuation to the sound energy both by its inherent loss mechanisms and high coefficient of reflection.

Coated Steel Plate

A 1/8 inch steel plate having a typical flame-sprayed coating of zirconium oxide on the emergent surface, is shown in Fig. 16D. As will be noted, the interaction of the sound beam is quite complex. In this case the Schlieren system was adjusted for maximum sensitivity. Consequently, much of the diffused portion of the sound beam, along with its associated reflections and refractions, are shown. Of primary interest in this photo is the bubble formation visible at the top of the incident surface and the very bright layer covering the emergent surface. The bubbles might be attributed to thermal effects and/or cavitation processes. The phenomenon that is occurring at the emergent surface may be due to the ceramic coating. It is known that zirconia coatings have a high porosity and, hence, are capable of entrapping air.

When this coating is excited by high intensity ultrasonic energy, the air may be caused to escape thereby producing the bright "blanket" on the surface. It will also be noted that the emergent sound beam is not uniform but consists of high and low intensity areas. This again, may be due to the loss mechanisms inherent in the ceramic coating.

EXPERIMENTAL OBSERVATIONS OF SPURIOUS RESULTS

In studies of the interaction of focussed sound with solids, spurious phenomena are observed. Typical spurious effects, shown in Fig. 16D, result when high intensity sound is transmitted through a zirconia coated steel plate. Examination of other materials, such as lead and Chromalloy W2 on molybdenum, using high intensity focussed ultrasonic energy, produced similar results as shown in Figs. 17 and 18. These phenomena are attributed to either thermal effects, cavitation, acoustic streaming or a combination of the effects. Since any one of these processes can alter the refractive index of the media in which they occur, (in this case the media is water), they will appear as spurious bright areas, bubble formations or apparent turbulence in the Schlieren image.

As stated previously, through the use of acoustic lenses we are able to produce high ultrasonic intensities. Consequently, if a material is lossy it would be conducive to the conversion of this sound energy into heat. The heat generated, although very small, would be sufficient to vary the refractive index of the water and, hence, appear as spurious interactions in the Schlieren photo. Furthermore, cavitation threshold pressure is dependent upon temperature as well as pressure, and the presence of nucleation centers. Hence, if the material has a rough or porous surface e.g. zirconium oxide, capable of entrapping air it is quite possible to produce intense cavitation at the surface of the material.

Acoustic streaming is normally associated with variations in energy density and high intensity sound fields. From previous discussions, it is obvious that our system fulfills the requirements necessary to produce streaming. Therefore, one might expect violent motion of suspended particles near the interface of the specimen when subjected to intense ultrasonic radiation. This particle motion would vary the refractive index of the water and thereby appear in the Schlieren photo.

It is felt that a more extensive study must be made of these phenomena before any final conclusions can be drawn. Although the effects could be detrimental in some tests, i.e. surface wave propagation, by the same token they may provide another means of non-destructive examination of bond structures. If one considers the thermal effects due to ultrasonic radiation, it might be feasible to excite infra-red detectors with energy provided by focussed sound beams in lossy materials.

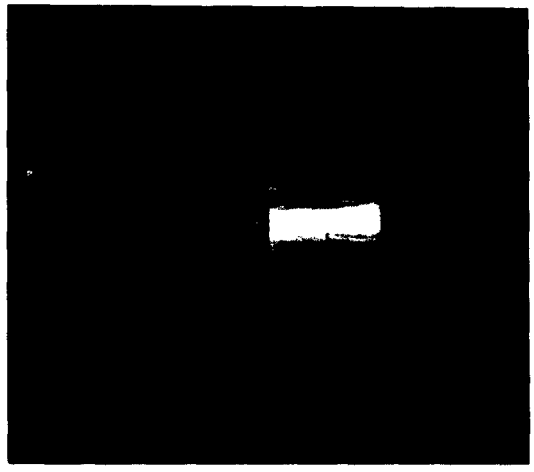

Fig. 17 - SPURIOUS EFFECTS ENCOUNTERED IN SOUND PROPAGATION THROUGH A HIGH LOSS MATERIAL. The sound beam is propagating from right to left.

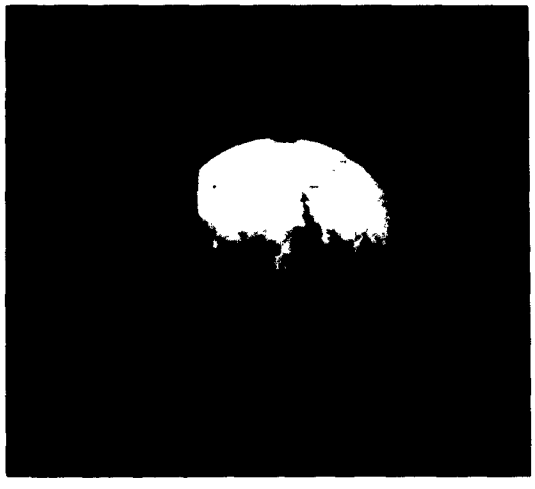

Fig. 18 - VARIATIONS IN THE OPTICAL REFRACTIVE INDEX PRODUCED BY MECHANISMS OTHER THAN THE SOUND BEAM.

Section IV

SURFACE WAVES

In developing suitable ultrasonic methods for the detection of defects in coating-substrate systems, the character of the defect being sought is of prime importance. A laminar type defect, for example, presents its largest cross sectional area parallel to a surface of the material in which it exists. Consequently, this type of defect is most readily detected with the use of transmission or reflection techniques, where compressional waves are propagated at normal incidence to the surface of the material. If the defect were to occur in the form of a crack normal to the surface, a minimum cross sectional area is presented to the surface and, hence, the above techniques would not provide sufficient detection sensitivity.

The geometrical orientation of a probable defect structure is, in general, dependent upon the physical properties of the system in which it exists. The diffusion coatings exhibit defects in the form of cracks, normal to the coating face and extending to the diffusion zone. These cracks may arise during diffusional growth or possibly as a result of stresses induced by thermal cycling, however, once a crack has penetrated the coating, oxidation of the substrate will occur. For some substrates the oxide requires a larger volume than does the metal. Consequently, the stress, generated by the replacement of metal by oxide, may pry the coating away from the substrate and thereby produce new cracks. These cracks can occur at the coating-substrate interface or may form normal to the interface and parallel with the original crack, depending upon the relative strengths of the bond and the coating.

Metallographic examination has shown that in several coating-substrate systems, the cracks are relatively narrow: a width of 250 micro-inches is typical. The cracks were found to penetrate through the entire coating which normally is about 0.003 inches thick. As discussed above, defects such as these would not be readily detected using normal incidence transmission techniques. The most feasible detection method employs surface waves, which inherently restrict the ultrasonic energy to a surface layer of approximately one wavelength thickness. This particular type of wave offers an additional advantage in that the energy propagates in a direction normal to the largest surface area presented by the crack. The emphasis on diffusion coatings has produced increased interest in surface wave generation and propagation. Although valid results have been reported[7] previously, they were empirical rather than theoretical. To

---

[7] WADD Technical Report 60-157, page 15 and WADD Technical Report 61-91, page 21.

permit the empirical investigations to proceed, it has become necessary to develop a theoretical framework to guide the experiments.

THEORY OF SURFACE WAVE GENERATION

The application of surface waves to the detection of surface defects has created a need for a better understanding of this type of elastic wave. The theory for shear and dilatational waves is readily available in texts on elastic theory, but the subject of Rayleigh waves has received much less extensive treatment. The following discussion is directed to clarifying the theory of surface wave generation in a solid and the effect on surface wave propagation of the elastic properties of the solid.

Throughout this discussion, the symbols listed on page vi are used. Standard conventions of notation are also followed, including the summation convention.

Elastic Constants

The theory of ultrasonic waves is based on elasticity theory. The initial point of this discussion is the definition of the elastic constants in terms of the stresses and the strains. For isotropic elastic materials, the stresses and the strains are related by:

$$p_{ii} = \lambda\theta + 2\mu \frac{\partial u_i}{\partial x_i} \qquad \text{(not summed over i)}$$

$$p_{ij} = \mu\left(\frac{\partial u_i}{\partial x_j} + \frac{\partial u_j}{\partial x_i}\right) \qquad (1)$$

where $i = 1, 2, 3$ and the displacement S is given by

$$\bar{S} = u_i \bar{e}_i \qquad \text{and } \theta \text{ is defined as}$$

$$\theta = \bar{\nabla} \cdot \bar{S}$$

In the absence of any body forces, the equations of particle motion, neglecting second order terms, are

$$\rho \frac{\partial^2 u_j}{\partial t^2} = \frac{\partial p_{ij}}{\partial x_i} \tag{2}$$

Using the definitions of $\bar{S}$ and θ, and Equations (1), the three Equations (2) may be combined into

$$\rho \frac{\partial^2 \bar{S}}{\partial t^2} = (\lambda + \mu) \bar{\nabla} \theta + \mu \bar{\nabla}^2 \bar{S} \tag{3}$$

It should be noted that the last term, $\mu \bar{\nabla}^2 \bar{S}$, implies $\mu \bar{\nabla} \cdot \bar{\nabla} \bar{S}$ and the operation $\bar{\nabla} \bar{S}$ produces a dyadic.

Compressional and Shear Waves

The strains in an elastic body are divided into dilatational and shear depending on whether the strain produces just a change in volume or just a distortion. In a similar manner, two types of elastic waves are distinguishable, dilatational waves and shear waves.[8] To orient the theory, it is convenient to introduce two displacement potentials, a scalar potential, ϕ, and a vector potential, $\bar{\Psi}$. Then

$$\bar{S} = \bar{\nabla} \phi + \bar{\nabla} \times \bar{\Psi} \tag{4}$$

By the definition of θ,

$$\theta = \bar{\nabla} \cdot \bar{S} = \bar{\nabla}^2 \phi \tag{5}$$

[8]Other types of waves are possible, but to obtain the theoretical results required, only the dilational and shear waves need to be considered here.

since the term containing the divergence of a curl is identically zero. Substituting for $\bar{S}$ and θ in Equation (3) produces an equation of motion in terms of the displacement potentials

$$\rho \frac{\partial^2}{\partial t^2} (\bar{\nabla} \phi + \bar{\nabla} \times \bar{\psi}) =$$

$$(\lambda + 2\mu) \bar{\nabla}^2 (\bar{\nabla} \phi) + \mu \bar{\nabla}^2 (\bar{\nabla} \times \bar{\psi}) \tag{6}$$

If the x-component only is considered, and the order of partial differentiation is reversed, then

$$\frac{\partial}{\partial x} \left(\rho \frac{\partial^2 \phi}{\partial t^2} \right) + \frac{\partial}{\partial y} \left(\rho \frac{\partial^2 \psi_z}{\partial t^2} \right) - \frac{\partial}{\partial z} \left(\rho \frac{\partial^2 \psi_y}{\partial t^2} \right)$$

$$= (\lambda + 2\mu) \frac{\partial}{\partial x} (\bar{\nabla}^2 \phi) + \frac{\partial}{\partial y} (\mu \nabla^2 \psi_z) \tag{6a}$$

$$- \frac{\partial}{\partial z} (\mu \nabla^2 \psi_y)$$

In a later stage of this discussion it will be assumed that all of the waves propagate in the x-z plane and the wave fronts are infinitely wide in the y-direction. This assumption allows the partial derivatives with respect to y to be equated to zero and provides that $\bar{\psi}$ will be parallel to the y-axis. Then:

$$\frac{\partial}{\partial x} \left[\rho \frac{\partial^2 \phi}{\partial t^2} - (\lambda + 2\mu) \nabla^2 \phi \right]$$

$$= \frac{\partial}{\partial z} \left[\mu \nabla^2 \psi_y - \rho \frac{\partial^2 \psi_y}{\partial t^2} \right] \tag{6b}$$

Two similar equations for the stresses in the other directions are also obtained by taking the y- and z- components. One possible solution of the equations is obtained by selectring ϕ and Ψ so that the following equations are satisfied.

$$\nabla^2\phi = \frac{1}{a^2}\frac{\partial^2\phi}{\partial t^2}$$

$$\nabla^2\psi_i = \frac{1}{\beta^2}\frac{\partial^2\psi_i}{\partial t^2} \qquad (7)$$

where $a = \left[(\lambda + 2\mu)/\rho\right]^{1/2}$ and $\beta = (\mu/\rho)^{1/2}$

The solution to Equation (7) may be written in the form

$$\left.\begin{aligned}\phi &= A_1 \exp\left[ik(ct - x + az)\right] + A_2 \exp\left[ik(ct - x - az)\right] \\ \Psi &= B_1 \exp\left[ik(ct - x + bz)\right] + B_2 \exp\left[ik(ct - x - bz)\right]\end{aligned}\right\} \qquad (8)$$

The form of the exponential in Equation (8) has been selected so as to facilitate a derivation of Snell's law. The first term in the equation for ϕ represents a wave travelling in the positive x- and negative z-directions so that the direction of propagation mades an angle e with the x-axis as in Fig. 19.

The constant, c, in the exponentials in Equations (8) represents the trace velocity[9] along the x-axis. If the x-axis represents the surface of a solid, new waves will be produced by reflection and refraction. If the boundary conditions at the surface of the solid are satisfied, the trace velocities along the x-axis of all incident, reflected and refracted waves

---

[9] T. F. Heuter and R. H. Bolt "Sonics" John Wiley and Sons, New York, 1955, page 73.

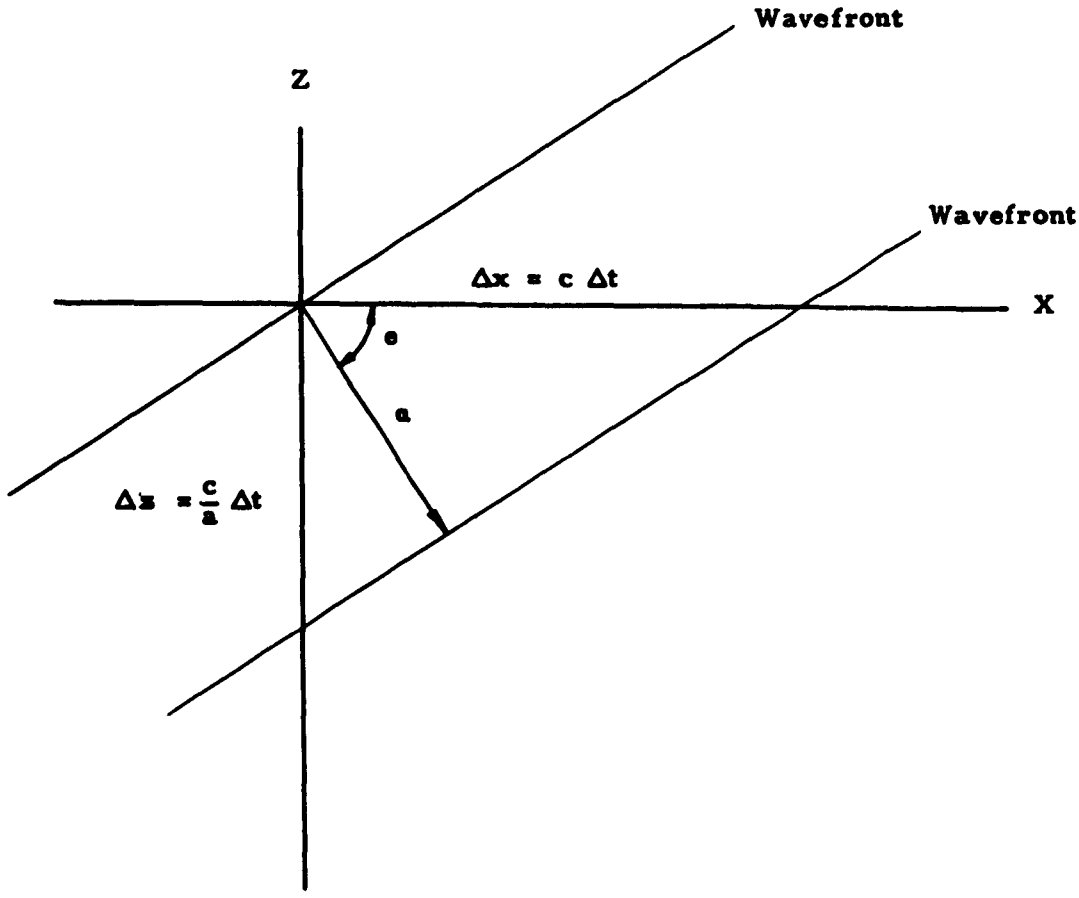

Fig. 19 - TRUE AND TRACE VELOCITIES OF A WAVE TRAVELLING OBLIQUELY TO THE AXES. The true velocity is a. The trace velocity along the X-axis is c and along the Z-axis is c / a.

must be equal. The equality of the trace velocities is a direct consequence of constructive interference, necessary for reflection or refraction.

Liquid-Solid Interface

Assume now that a dilatational wave is incident, from the liquid side, upon a liquid-solid interface. In the liquid, μ and β are both zero if the liquid has negligibly low viscosity. In general then, there will be an incident and reflected compressional wave in the liquid and a refracted shear wave and a refracted compressional wave in the solid. Because of the absence of shear components in the liquid, no vector potential is required for the liquid.

The direction of the waves is illustrated in Fig. 20.

The boundary conditions to be satisfied at the interface (assumed to be the x-y plane) are:

$$\begin{aligned} u &= u' \\ w &= w' \\ p_{zz} &= p_{zz}' \\ p_{zx} &= 0 \end{aligned} \qquad (9)$$

when $x = y = 0$ and

where the unprimed quantities apply to the liquid and the primed quantities to the solid.

It will be assumed that solutions for the displacement potentials in both liquid and solid will be of the form shown in Equations (8). If the boundary conditions can be satisfied, then equality of the trace velocities of all waves is assured. The assumed solutions for the potentials will be:

$$\begin{aligned} \phi &= A_1 \exp\left[ik(ct - x + az)\right] + A_2 \exp\left[ik(ct - x - az)\right] \\ \phi' &= A' \exp\left[ik(ct - x + a'z)\right] \\ \psi' &= B' \exp\left[ik(ct - x + b'z)\right] \end{aligned} \qquad (10)$$

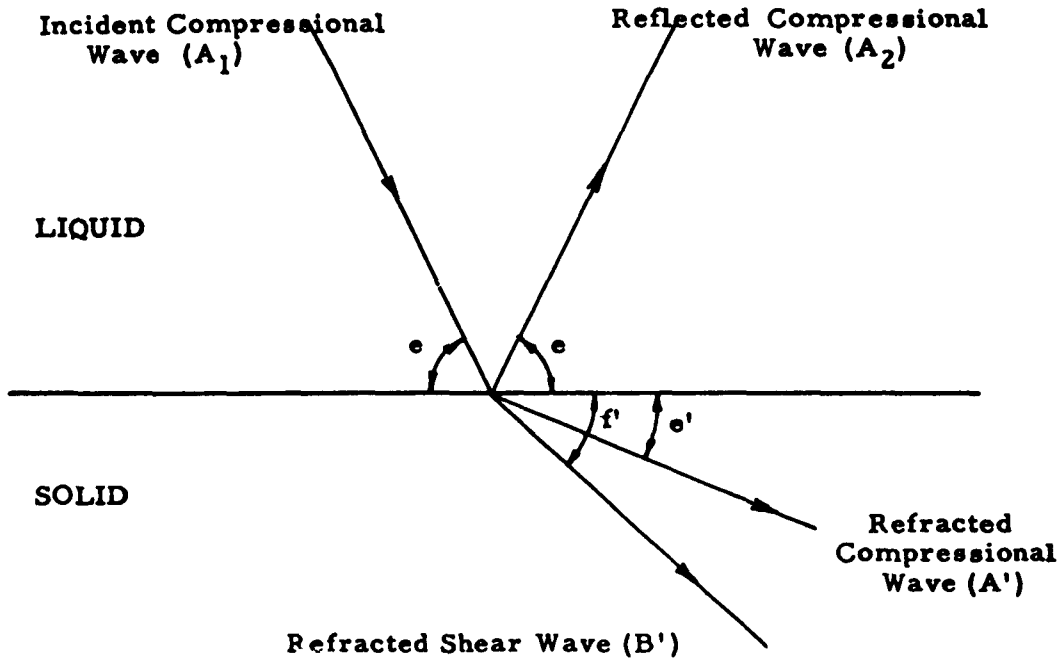

Fig. 20 - WAVES PRESENT WHEN A COMPRESSIONAL WAVE IS INCIDENT FROM THE LIQUID ONTO A LIQUID-SOLID INTERFACE. The letters A_1, A_2 and A' are the amplitudes of the scalar displacement potentials associated with each of the compressional waves. B' is the amplitude of the vector potential associated with the refracted shear wave.

Using Equations (1) and (4) and substituting into the boundary conditions, Equations (9), produces four new equations:

$$
\begin{aligned}
A_1 + A_2 &= A' + b'B' \\
a(A_1 - A_2) &= a'A' - B' \\
\lambda(1 + a^2)(A_1 + A_2) &= \lambda'(1 + a'^2)A' + 2\mu'\left[a'^2 A' - b'B'\right] \\
2a'A' + (b'^2 - 1)B' &= 0
\end{aligned}
\tag{11}
$$

Assuming that solutions can be found for A_2, A' and B' in terms of A_1 and the remaining constants, then the equality of the trace velocities is assured. By examining the relationship between the trace velocities and the actual velocities it can be shown that

$$
c = \frac{\alpha}{\cos e} = \frac{\alpha'}{\cos e'} = \frac{\beta'}{\cos f'} \tag{12}
$$

Since α and β are the dilatational and shear velocities and the angles e and f are the complements of the incident or refractive angles, it is obvious that Equation (12) is an alternate form of Snell's Law.

The constants a, a' and b' in Equation (10) are related to the angles e, e' and f' by

$$
\begin{aligned}
a &= \tan e \\
a' &= \tan e' \\
b' &= \tan f'
\end{aligned}
\tag{13}
$$

These equations may be determined from the relationship between trace and true velocities.

Equations (11) may be solved and the results simplified using Equations (12) and (13). The solutions are

$$\begin{aligned} A_2/A_1 &= -\left[\rho c^2 a'(b'^2+1) + \mu' a(b'^2-1) + 4a'b'\right] / D \\ A'/A_1 &= 2\rho e^2 a(b'^2-1) / D \\ B'/A_1 &= 4\rho a a' c^2 / D \end{aligned} \qquad (14)$$

$$\text{where } D = \rho c^2 a'(b'^2+1) + \mu' a\left[(b'^2-1)^2 + 4a'b'\right]$$

Surface Waves

The relative amplitudes and directions of all waves are determined by the ratios of the amplitude of the potentials given in Equations (14) and by Snell's Law, Equations (12). Since α, α' and β' in Equations (12) are fixed by the elastic constants of the liquid and the solid, and since c can be made any value larger than α, then $\cos e'$ and $\cos f'$ can be made larger than unity for some values of e. This demands that e' and f' be pure imaginary and a' and b' are also pure imaginary.

The scalar and vector potentials for the solid then have the form

$$\left.\begin{aligned} \phi' &= A' \exp(a''z) \exp\left[ik(ct - x)\right] \\ \psi' &= B' \exp(b''z) \exp\left[ik(ct - x)\right] \end{aligned}\right\} (15)$$

where $ia'' = a'$ and $ib'' = b'$ and a'' and b'' are real.

Substituting in Equation (4) for $\bar{S}$ and extracting the x and z components of displacement gives the results for the particle displacements at the interface:

$$\left.\begin{aligned} u' &= -(ikA' + b''B') \exp\left[ik(ct - x)\right] \\ w' &= -(a''A' + ikB') \exp\left[ik(ct - x)\right] \end{aligned}\right\} (16)$$

These equations can be rewritten by letting

$$-ikA' - b''B' = E \exp i\zeta$$
$$-a''A' + ikB' = F \exp i\xi \qquad (17)$$

Then

$$u' = E \exp i(wt - kx + \zeta)$$
$$w' = F \exp i(wt - kx + \xi) \qquad (18)$$

The last equations show that the particle motion at the surface has components normal to and parallel with the interface and that the two components are out of phase. In general, the particle motion will be elliptical. Equations (15) show that the motion decays exponentially with depth below the surface of the solid.

Propagation of Surface Waves Along a Liquid-Loaded Surface

The equations relating the amplitudes of the potentials of the surface wave to the potential of the compressional wave in the liquid were derived for the region of the interface where the compressional wave is incident upon the surface. The only wave that can be propagated in the liquid away from the region is a reflected compressional wave. However, the solid can support a surface wave, which can then propagate out of the region where it was generated. Since the propagated surface wave contains a component of displacement normal to the interface, some of the energy of this wave will be transferred to the liquid. This reradiated energy will be in the form of a compressional wave which is in the form of a beam oriented parallel to the reflected compressional wave. Boundary conditions will have to be satisfied, and these conditions can be satisfied only if the amplitudes of the reradiated compressional wave in the liquid, and the amplitudes of this surface wave in the solid, are related by the elastic constants of the two media. If the boundary conditions can be satisfied only for a compressional wave with a high amplitude compared to the surface wave amplitude, the effective attenuation to the surface wave will be high and the wave will propagate along the interface only a short distance.

Discussion of Theory

The theoretical discussion has served several purposes. The results provide a framework for experiments using surface waves and predict the conditions under which surface waves will be generated at a liquid-solid interface. The most important consideration is the angle of incidence of the compressional wave. The verification of Snell's Law provides a means of calculating the "critical" angle at which energy from an incident compressional wave is transferred to a surface wave. The theory, moreover, provides a knowledge of the propagation of a surface wave, and details the particle motion. Although this discussion has assumed an infinitely wide compressional beam, and consequently no information is available on beam spreading of a surface wave, the theory does form a basis for more inclusive theory which could be directed towards finite beam widths. The theory can also be extended to solid-solid interfaces and can be used to determine optimum design of transducers for generating surface waves in solids.

EXPERIMENTAL APPLICATION OF SURFACE WAVE THEORY

Theory shows that the amplitude of a Rayleigh wave decays exponentially with depth penetration in a solid. For typical metals, such as aluminum or steel, the decay constant has a value such that the wave amplitude, at a depth of one wavelength below the surface, is about 5 percent of the amplitude at the surface. The energy, propagated in a layer extending from the surface to a depth D, can be calculated by the equation:

$$E = I_o \int_0^D \exp(-2\alpha z)\, dz$$

where I_o is the intensity at the surface and α is the amplitude decay constant. Hence, it may be shown that more than 99 percent of the total wave energy is propagated in a layer one wavelength thick. Furthermore, at an ultrasonic frequency of 7 Mc/s, the wavelength of a Rayleigh wave is about 0.018 inches. Consequently, a crack extending 0.003 inch in depth or approximately 1.6 wavelength, will intercept about 60 percent of the total energy in the surface wave. The above approximate calculations are sufficient to show that even shallow cracks, existing normal to the surface, will reflect an appreciable portion of a surface wave and, hence, attenuation measurements should constitute a very sensitive method for the detection of cracks.

If the depth of a crack is comparable to a wavelength, then theory shows that almost complete reflection of a Rayleigh wave will occur. Hence, reflection techniques may then be used to detect these deeper cracks.

The apparatus shown in Fig. 21 was designed to measure surface wave attenuation in both homogeneous and nonhomogeneous materials. The basic system consists of a slide assembly to permit controlled longitudinal motion of a flat plate specimen. Surface waves are generated at one end of the specimen, using a 7 Mc/s, x-cut quartz crystal and a lucite wedge transducer. The angle of the wedge is such that Snell's Law is satisfied for the particular material under investigation. The generating transducer is mechanically fastened to the specimen, with a suitable couplant at the transducer-specimen interface, to maintain constant coupling throughout the investigation. Approximately half the apparatus is then submerged in a water tank as shown in Fig. 22, and the surface wave propagates along the plate until it reaches the immersed region of the specimen. At this liquid-solid interface the energy is reradiated, through mode conversion, into the water as a compressional wave. This wave emerges from the specimen at an angle that must also satisfy Snell's Law. The emergent compressional wave is detected by the submerged receiver, whose angle of incidence is adjustable relative to the surface of the specimen.

Since a Rayleigh wave can propagate an appreciable distance only along a free surface, the free path length of the wave propagation can be reduced by increased immersion of the specimen in the water. By maintaining a constant voltage across the surface wave generator and measuring the change in received signal amplitude as the path length is varied, surface wave attenuation data is obtained.

Initial experiments with this apparatus, and a homogeneous steel plate specimen showed, that although surface waves were detected at the predicted orientation of the submerged receiver, spurious sound energy was also present over a wide range of receiver orientations.

Previous measurements[10] have shown that the incident angle of a compressional wave with a solid, can be varied over only a very small range (one or two degrees) and still generate a surface wave. Hence, spurious sound energy, present at other than the critical angle, is due to the reradiation of random compressional and/or shear waves that have been coupled into the specimen.

In an idealized system, all incident compressional energy would undergo complete mode conversion at the transducer-solid interface and, hence, only a surface wave would propagate in the specimen. However, in a practical system where an acoustic impedance mismatch occurs at the interface, some of the incident energy is reflected back into the wedge transducer. Due to the geometrical configuration of the wedge, multiple internal reflections occur and produce sound beams incident on the interface at incorrect angles of

---

[10] WADD Technical Report 61-91, Part 1, page 21.

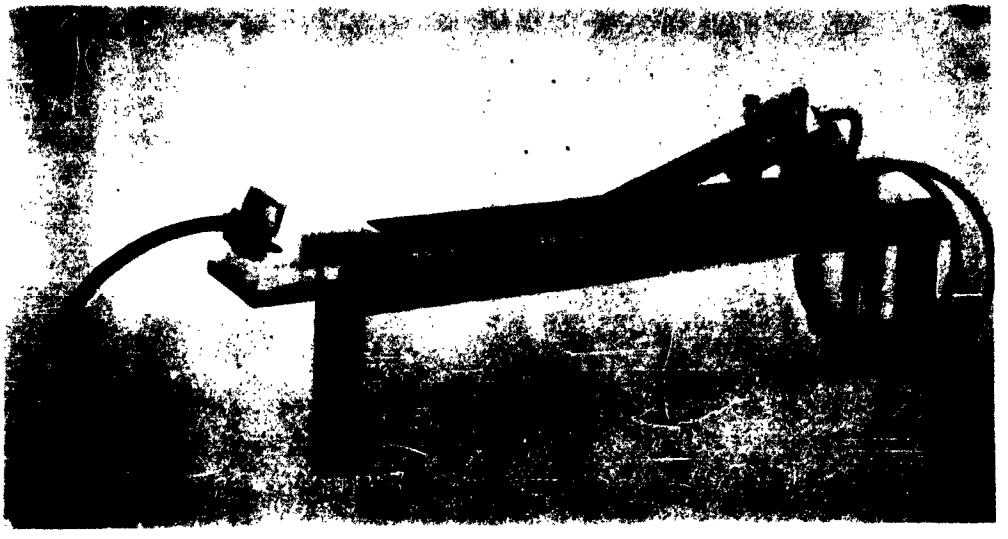

Fig. 21 - TRANSDUCER CONFIGURATION FOR SURFACE WAVE APPARATUS. A lucite wedge with a 7 Mc/s, x-cut quartz crystal, is fixed to the specimen and used to generate a surface wave. The receiver can be varied through an angle of 90° to 12° relative to the specimen surface.

Fig. 22 - EXPERIMENTAL APPARATUS FOR THE MEASUREMENT OF SURFACE WAVE ATTENUATION. The receiver end of the apparatus is submerged in the water tank. The specimen is moved longitudinally into and out of the water. Changes in amplitude of the received pulse, as the specimen is moved, correspond to variations in attenuation associated with the changing surface wave path length.

incidence to produce surface waves. Experiments have shown that additional shear and compressional energy is coupled into the specimens. Hence, the specimen acts as a sound generator and reradiates spurious compressional energy into the water at random angles. This condition was corrected through the use of a carefully constructed isosceles triangle transducer for the generation of surface waves.

Additional investigation of surface wave attenuation, using the triangular generator, has been conducted on an oil hardened steel plate. Measurements indicate that the surface wave is attenuated about 2-1/2 db over a free path length of 6 inches.

Measurements relating surface wave attenuation to crack concentration in diffusion coatings have not been completed as yet, however, work is still progressing along these lines.

To illustrate the effect of surface damping on the amplitude of a Rayleigh wave, Figs. 23 and 24 are presented. The pulse shown in Fig. 23 is the received signal, produced by the reradiated compressional wave, as a result of a Rayleigh wave propagated along the free surface of the steel plate. A very thin layer of petroleum jelly, approximately 1/16 inch wide, was applied to the surface of the specimen traverse to the direction of propagation. Figure 24 shows the corresponding decrease in signal amplitude as a result of this damping.

Section V

SUMMARY AND CONCLUSIONS

Two dimensional images of 1/8, 1/16, and 1/32 inch diameter laminar defects, in zirconia-inconel bonds, have been obtained with the use of an acoustic image converter system as a result of exploitation of the charge scanning technique. The acoustic sensitivity and resolution of this system is such that defect thicknessess of 300 to 500 microinches, or about a factor of three greater than the average large grains in the coating material, are detectable.

New coating techniques have been developed to produce realistic defects at the interface of ceramic-metal bonds. Examination of these defect structures, by various ultrasonic techniques, provides a true evaluation of acoustic sensitivity and resolution for a given method.

The combination of Schlieren optics and focussed ultrasonic energy has provided a visual means of investigating the properties of sound fields and the interaction of a high intensity sound beam with a solid. A

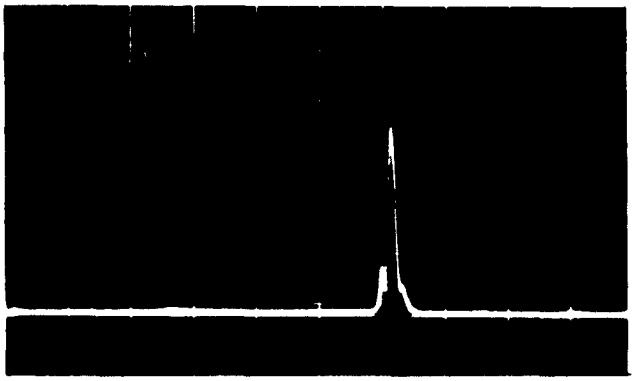

Fig. 23 - SIGNAL PRODUCED BY MODE CONVERSION OF A SURFACE WAVE TO A COMPRESSIONAL WAVE AT A LIQUID - SOLID INTERFACE. The submerged receiver in Fig. 21 detects compressional energy re-radiated into the liquid after transmission as a surface wave along the steel plate.

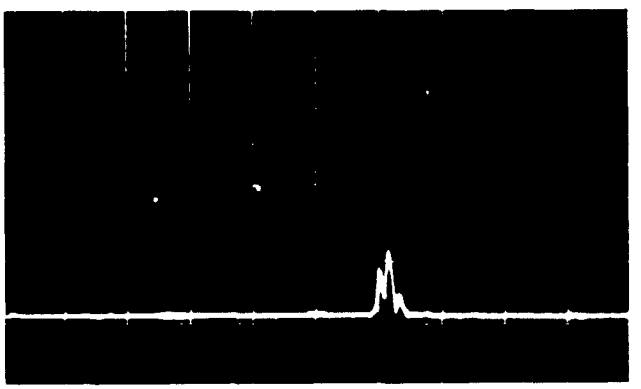

Fig. 24 - EFFECT OF DAMPING ON SURFACE WAVE PROPAGATION IN A STEEL PLATE. A small amount of petroleum jelly was applied to the surface of the steel plate in Fig. 22. The resulting change in signal amplitude, as compared to Fig. 22, is due to damping of the surface.

qualitative analysis of transmitted sound through a solid, has been presented. The effect of elastic and dissipative properties of various materials is graphically illustrated by Schlieren photographs. Additional phenomena, attributed to either thermal effects, sonic cavitation, or acoustic streaming were noted when high intensity focussed sound was used. Further investigations, to determine the effect of these phenomena on defect detection, are still necessary.

The theory of Rayliegh wave generation and propagation was reviewed to provide a guide for further experimental work. Application of the theory has dictated the design of surface wave generators and experimental apparatus. It also has been used to show that even shallow cracks, occurring normal to a surface, will markedly attenuate Rayliegh waves.

Experimental apparatus has been constructed to measure surface wave attenuation and measurements have been made in homogeneous materials. Further experiments are required to relate surface wave attenuation to surface crack density.

Aeronautical Systems Division, Dir/Materials and Processes, Metals and Ceramics Lab, Wright-Patterson AFB, Ohio.
Rpt No. ASD TR 61-91, Pt II. ULTRASONIC METHODS FOR NONDESTRUCTIVE EVALUATION OF CERAMIC COATINGS. Final report, Feb 63, 44pp. incl illus.

Unclassified Report

This report describes investigations into the use of ultrasonic techniques to determine the strength and integrity of ceramic-metal bonds. An acoustic image converter system was used successfully to obtain a television type display of 1/32 in. diameter laminar defects in a zirconium

(over)

oxide-inconel bond. The measured defect thickness varied between 300 and 500 microinches or about a factor of three greater than the average large grain in the coating material. Schlieren optical and acoustic lens techniques were used to visually investigate detailed properties of ultrasonic fields and the interaction of ultrasonic energy with a solid. The theory of Rayleigh waves was reviewed to provide a framework for experimental integrity determinations of ceramic coatings.

1. Ultrasonic test methods
2. Ceramic coating
I. AFSC Project 7360, Task 736002
II. Contract No. AF 33(616)-6396
III. Armour Research Foundation of Ill. Institute of Technology, Chicago 16, Illinois.
IV. K. E. Feith
W. E. Lawrie
V. Aval fr OTS
VI. In ASTIA collection

Aeronautical Systems Division, Dir/Materials and Processes, Metals and Ceramics Lab, Wright-Patterson AFB, Ohio.
Rpt No. ASD TR 61-91, Pt II. ULTRASONIC METHODS FOR NONDESTRUCTIVE EVALUATION OF CERAMIC COATINGS. Final report, Feb 63, 44pp. incl illus.

Unclassified Report

This report describes investigations into the use of ultrasonic techniques to determine the strength and integrity of ceramic-metal bonds. An acoustic image converter system was used successfully to obtain a television type display of 1/32 in. diameter laminar defects in a zirconium

(over)

oxide-inconel bond. The measured defect thickness varied between 300 and 500 microinches or about a factor of three greater than the average large grain in the coating material. Schlieren optical and acoustic lens techniques were used to visually investigate detailed properties of ultrasonic fields and the interaction of ultrasonic energy with a solid. The theory of Rayleigh waves was reviewed to provide a framework for experimental integrity determinations of ceramic coatings.

1. Ultrasonic test methods
2. Ceramic coating
I. AFSC Project 7360, Task 736002
II. Contract No. AF 33(616)-6396
III. Armour Research Foundation of Ill. Institute of Technology, Chicago 16, Illinois.
IV. K. E. Feith
W. E. Lawrie
V. Aval fr OTS
VI. In ASTIA collection